Maytansinoid-Antibody Conjugates Induce Mitotic Arrest by Suppressing Microtubule Dynamic Instability

Emin Oroudjev[1], Manu Lopus[1], Leslie Wilson[1], Charlene Audette[2], Carmela Provenzano[2], Hans Erickson[2], Yelena Kovtun[2], Ravi Chari[2], and Mary Ann Jordan[1]

Abstract

Maytansine and its analogues (maytansinoids) are potent microtubule-targeted compounds that inhibit proliferation of cells at mitosis. Antibody-maytansinoid conjugates consisting of maytansinoids (DM1 and DM4) attached to tumor-specific antibodies have shown promising clinical results. To determine the mechanism by which the antibody-DM1 conjugates inhibit cell proliferation, we examined the effects of the cleavable anti-EpCAM-SPP-DM1 and uncleavable anti-EpCAM-SMCC-DM1 conjugates on MCF7 human breast tumor cells. We also examined the effects of the free maytansinoids, maytansine and *S*-methyl DM1 (a version of DM1 that is stable in cell culture medium), for comparison. Both the conjugates and free maytansinoids potently inhibited MCF7 cell proliferation at nanomolar and subnanomolar concentrations, respectively, by arresting the cells in mitotic prometaphase/metaphase. Arrest occurred in concert with the internalization and intracellular processing of both conjugates under conditions that induced abnormal spindle organization and suppressed microtubule dynamic instability. Microtubule depolymerization occurred only at significantly higher drug concentrations. The results indicate that free maytansinoids, antibody-maytansinoid conjugates, and their metabolites exert their potent antimitotic effects through a common mechanism involving suppression of microtubule dynamic instability. *Mol Cancer Ther; 9(10); 2700–13. ©2010 AACR.*

Introduction

Maytansine and its analogues (Fig. 1) are benzoansamacrolides (1–3) that show powerful antimitotic activity (4, 5). Maytansine (Fig. 1) is a microtubule-targeted drug that binds to tubulin at the *Vinca* binding site (6, 7). Similar to *Vinca* alkaloids, maytansine can depolymerize microtubules and arrest cells in mitosis (8–10). However, maytansine displays almost 100 times higher cytotoxicity in cells than the *Vinca* alkaloids (11).

In human clinical trials, maytansine showed a small therapeutic window due to neurotoxicity and to adverse effects on the gastrointestinal tract (11). However, the powerful cytotoxicity of maytansinoids could make them valuable for anticancer therapies using tissue-specific drug delivery approaches, particularly as antibody-maytansinoid conjugates (AMC; refs. 12–16). Preclinical studies indicate that AMCs have significantly improved potential as anticancer agents compared with the unconjugated maytansinoids (17–19). Clinical trials using several different AMCs have been conducted (20–22). A recent trial on trastuzumab-DM1 (T-DM1), a maytansinoid conjugated to the anti–human epidermal growth factor receptor 2 therapeutic antibody trastuzumab, showed good efficacy in metastatic breast cancer (23). Moreover, the CD56-targeting AMC, lorvotuzumab-mertansine, has shown promising results in solid and liquid tumors that express CD56 (24). T-DM1 (trastuzumab-MCC-DM1) utilizes a nonreducible thioether-based linker, whereas lorvotuzumab mertansine (huN901-SPP-DM1) utilizes a disulfide-based linker (Fig. 1).

The optimal linker for an AMC is selected by preparing conjugates with a panel of linkers and evaluating their activity *in vitro* and in human tumor xenograft models. The conjugate with the most antitumor activity and the widest therapeutic window, as defined by the difference between the maximum tolerated dose and minimally effective dose, is then selected. Preclinical studies (25, 26) with anti-CanAg (tumor-associated protein CA242)–targeting AMCs showed that the huC242 antibody component of cleavable disulfide-linked huC242-SPP-DM1 and the uncleavable huC242-SMCC-DM1 conjugate is proteolytically degraded in targeted cancer cells following antigen-mediated internalization and vesicular trafficking to the lysosomes to yield lysine-SPP-DM1 and lysine-SMCC-DM1 metabolites, respectively. The lysine-SPP-DM1 derived from the disulfide-linked conjugate

Authors' Affiliations: [1]Department of Molecular, Cellular, and Developmental Biology, and the Neuroscience Research Institute, University of California Santa Barbara, Santa Barbara, California, and [2]ImmunoGen, Inc., Waltham, Massachusetts

Corresponding Author: Mary Ann Jordan, Department of Molecular, Cellular, and Developmental Biology, and the Neuroscience Research Institute, University of California, Santa Barbara, CA 93106-9610. Phone: 805-893-5317; Fax: 805-893-4724. E-mail: jordan@lifesci.ucsb.edu

doi: 10.1158/1535-7163.MCT-10-0645

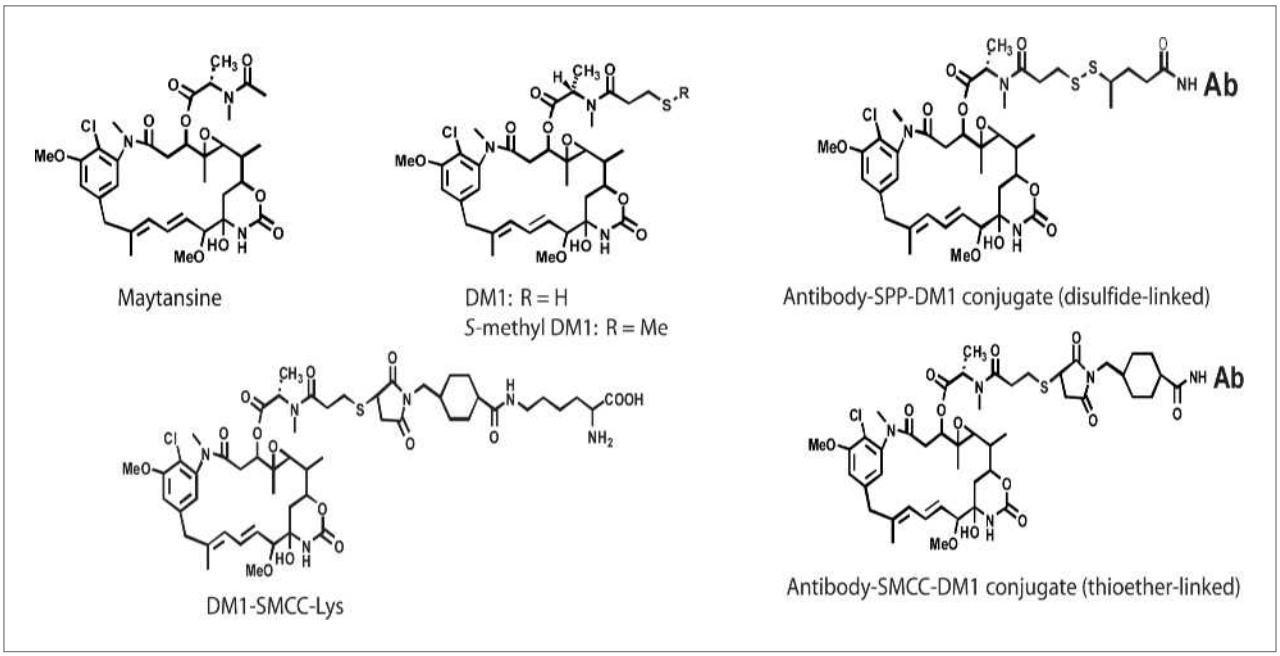

Figure 1. Structures of maytansine, DM1, and *S*-methyl DM1 (for DM1: R = H; for S-methyl DM1: R = Me), DM1 immunoconjugates, DM1-SMCC-lys metabolite.

undergoes further intracellular reduction to yield DM1 (25, 26). Formation of the hydrophobic DM1 metabolite is proposed to explain the bystander cell killing activity of huC242-SPP-DM1 that was observed in human tumor xenograft models (19). Microtubules are polymers composed of the protein tubulin that play a major role in mitosis and other important cell functions (27).

Microtubules are highly dynamic polymers, and their dynamics are tightly controlled both spatially and temporally in cells. In one type of dynamics, dynamic instability, the ends of the microtubules alternate between phases of growth and shortening. Recent research shows that many microtubule-targeted compounds, including the *Vinca* alkaloids, suppress dynamic instability, and they do so at concentrations significantly lower than those required to depolymerize microtubules. Suppression of dynamic instability plays a major role in the antimitotic effects of these drugs (27–29).

In an accompanying article, we report that maytansine and *S*-methyl DM1 (DM1-Me) bind to soluble tubulin with similar affinities (K_D values of 0.86 and 0.93 μmol/L, respectively), and that they inhibit microtubule polymerization with similar potencies (IC_{50} values of 1 and 4 μmol/L, respectively). Using purified bovine brain microtubules *in vitro*, we found that at a concentration of 100 nmol/L, the maytansinoids suppress dynamic instability by binding with high affinity to a small number of sites at microtubule ends (30). For example, we found that *S*-methyl DM1 binds to 37 saturable sites on microtubules with a K_D of 0.1 ± 0.05 μmol/L and to a large number of low-affinity sites on microtubules and sedimentable aggregates with a K_D of 2.2 ± 0.2 μmol/L. Thus, their affinity for tubulin at microtubule ends is 20-fold stronger than their affinity for free tubulin.

To understand the mechanism of action of the antibody-conjugated maytansinoids, we investigated the concentration- and time-dependent effects of maytansine, *S*-methyl DM1, and anti–EpCAM-DM1 conjugates on proliferation, G_2-M arrest, microtubule organization, and dynamic instability in MCF7 cells. Although antibody-DM1 conjugates were prepared with the thiol-containing maytansinoid DM1, we found that DM1 can oxidize in aqueous solution to produce a DM1 disulfide dimer or undergo disulfide exchange with cysteine in cell culture medium to give a mixed disulfide. Thus, we used the stable DM1 methyl thioether derivative (*S*-methyl DM1) in these studies. We found that the antibody-DM1 conjugates, maytansine, *S*-methyl DM1, and the intracellular metabolites of the antibody-DM1 conjugates all inhibit proliferation and induce mitotic arrest in association with suppression of microtubule dynamic instability.

Materials and Methods

Materials

All chemicals and materials were purchased from Sigma unless otherwise noted. Ultima Gold scintillation fluid was from Perkin-Elmer Life and Analytical Sciences. The high performance liquid chromatography (HPLC) 10 μm C-18 column (0.46 × 25 cm, Vydac) was obtained from the Nest Group. Maytansine was prepared as described previously (17, 31) and stored as aliquots of

1 mmol/L stock solutions in DMSO at −70°C. DM1 and tritium-labeled DM1 were prepared from ansamitocin P-3 and [^{3}H]ansamitocin P-3, respectively (26). *S*-[^{3}H]methyl-DM1 was prepared at American Radiochemicals by reacting DM1 with [^{3}H]methyl iodide. Stock solutions were diluted in DMSO to 1 μmol/L and further diluted in cell culture medium or buffer to the desired concentration, with no more than 1:10 dilution at each step. Antibody-DM1 and antibody-[^{3}H]DM1 conjugates were prepared as described elsewhere (32). The chimeric anti-EpCAM monoclonal antibody B38.1 and the non targeting anti-CD56 antibody were produced at ImmunoGen. Conjugates are described by including the abbreviation for the linkers used in conjugation. The ratio of DM1 molecules linked per antibody molecule was determined as previously described (32) and ranged from 3.5 to 4. AMC concentrations are expressed as the concentration of antibody rather than of the conjugated maytansinoid.

Cell culture

MCF7 human breast carcinoma cells stably expressing enhanced green fluorescent protein (EGFP)-α-tubulin (33) were used for all experiments and are referred to as MCF7 cells. The EGFP-α-tubulin–expressing cells were morphologically indistinguishable from unmodified MCF7 (acquired from the American Type Culture Collection), but the doubling time was increased by 20%. They were free of *Mycoplasma* as determined by Hoechst 33342 stain (Life Technologies) and MycoAlert *Mycoplasma* detection kit (Lonza). The expression level of EpCAM was identical on both unmodified MCF7 and EGFP-α-tubulin–expressing MCF7 cells (as verified by binding of muB38.1 antibody).

MCF7 cells were cultured as adherent cells in high glucose (4 g/L) and 25 mmol/L HEPES-fortified DMEM supplemented with 1× nonessential amino acids and 10% fetal bovine serum (Hyclone), and 0.5 mg/mL G418 (Biowhittaker) at 37°C in 5.8% CO_2. Cells were transferred into medium lacking G418 72 hours before the experiments.

Cell proliferation

Proliferation was measured by a modified sulforhodamine B assay (34). MCF7 cells were seeded at 2×10^4 per well in 96-well plates and incubated for 24 hours to allow cell attachment and recovery. Medium with or without maytansinoid was then added for a 72-hour incubation. Cells were fixed, stained, and the optical density (OD) of each well was determined (490 nm; Victor^{3}V Wallac 1420 Spectrophotometer, Perkin-Elmer). The percentage of inhibition of cell proliferation was calculated as follows: 100 − [100 (OD sample at 72 hours − OD control at 0 hour)/(OD control at 72 hours − OD control at 0 hour)]. The 50% proliferation inhibitory concentrations (antiproliferative IC_{50}) were calculated by fitting the concentration-response data with a sigmoid function using IGOR Pro 6.0 software (WaveMetrics). Triplicates of each condition were tested in each experiment. Results are mean and SEM of at least three independent experiments.

Cell cycle and mitotic index

MCF7 cells were seeded at 6×10^4 per 2 mL into six-well plates. After a 24-hour recovery period, fetal bovine serum (FBS) was reduced to 2% for another 24 hours (to duplicate the conditions used for imaging dynamic microtubules), then cells were incubated for 24 hours in culture medium with 10% FBS ± maytansinoid. Floating and adherent cells were collected, combined, concentrated by centrifugation, fixed, permeabilized with ice-cold 70% ethanol, washed with PBS, and stained with a Guava Cell Cycle Reagent (Guava Technologies) according to the manufacturer's protocol. The DNA content of ≥3,000 cells was measured by flow cytometry on Guava EasyCyte for each condition. Cell cycle distribution was analyzed by ModFit software (Verity Software House). Results are the mean and SEM of at least three independent experiments.

MCF7 cells were grown attached to coverslips pretreated with poly-L-lysine (400 μg/mL) or in six-well tissue culture plates and incubated with compound as in the cell cycle experiments. Cells (either on coverslips or detached from six-well plates by trypsinization) were fixed with 3.7% formaldehyde, stained with Alexa Fluor 488–conjugated anti-phosphohistone H3 antibody (Cell Signaling Technology), and imaged by immunofluorescence microscopy as described below. The proportion of cells that were positive for phosphorylated H3 histone (a mitotic marker) was measured by flow cytometry on Guava EasyCyte (Guava Technologies) or by microscopy on the Nikon Eclipse E800 (Nikon) microscope. The half-maximal mitotic arrest concentrations (IC_{50}) were calculated as described above.

Immunofluorescence microscopy

Cells were seeded on coverslips as above, incubated with maytansinoid for 24 hours, and fixed with 3.7% formaldehyde. Microtubules were stained with mouse monoclonal α-tubulin antibody (DM1A, Sigma-Aldrich) and FITC-conjugated goat anti-mouse antibody (Cappel MP Bio chemicals). Centrosomes were stained with rabbit polyclonal anti-pericentrin antibody (AB4448, Abcam) and rhodamine-conjugated goat anti-rabbit antibody (Cappel MP Biochemicals). Actin filaments were stained with rhodamine-conjugated phalloidin (Invitrogen). Cells were mounted with 4′,6-diamidino-2-phenylindole–containing Prolong Gold (Invitrogen). Microscopy was done on a spinning disc confocal microscope Olympus IX81 DSU (Olympus). Images were taken by ImagEM camera (Hamamatsu) under the control of the SlideBook software (Olympus).

Uptake of *S*-[^{3}H]methyl-DM1 by MCF-7 cells

To measure uptake of *S*-methyl DM1, MCF7 cells (2×10^5/mL) were incubated with 780 pmol/L *S*-[^{3}H]-methyl-DM1 (specific activity ~500 mCi/mmol), at 37°C for 7 hours. At each 1-hour time point, 1 mL of sample was harvested, cells were separated from the supernatant by centrifugation, and the supernatant was transferred to a 1 mL Eppendorf tube. Each cell pellet was washed with

10 mL culture medium. Cells were pelleted by centrifugation and lysed with 400 μL of lysis buffer [50 mmol/L Tris (pH 8.0), 200 mmol/L NaCl, 15 mmol/L EDTA, and 1% v/v Triton X-100]. Radioactivity in lysed cell pellets and supernatants were counted using a Packard Tri-Carb 2900 TR liquid scintillation analyzer.

Extraction of [^{3}H]maytansinoid metabolites following exposure of MCF-7/GFP cells to B38.1-[^{3}H]DM1 conjugates *in vitro*

Cultures of MCF-7/GFP cells (9×10^6) were exposed to 10 nmol/L Ab-[^{3}H]DM1 conjugates and incubated at 37°C for 5, 9, or 24 hours. The cells were harvested with trypsin, washed with PBS, and resuspended in 0.3 mL TBS. The cells treated with the disulfide-linked B38-SPP-[^{3}H]DM1 were additionally treated with 5 mmol/L *N*-ethyl maleimide at room temperature for 30 minutes to alkylate thiol groups. The cell suspensions were assayed for maytansinoid metabolites by HPLC and liquid scintillation counting following acetone extraction as previously described (25).

Live cell imaging and analysis of microtubule dynamic instability

Analysis of microtubule dynamic instability was done as described previously (33, 35), with minor modifications. MCF7 cells were seeded (6×10^4/2 mL) on coverslips coated with poly-L-lysine, laminin, and fibronectin in six-well plates. Cells were incubated for 24 hours in culture medium with 10% FBS and then for 24 hours in culture medium with 2% FBS to induce flattening, after which maytansinoid was added at the desired concentration. To control for potential rapid loss of drug from cells upon transfer to the imaging medium (cell culture medium lacking sodium bicarbonate and phenol red, but buffered with 25 mmol/L HEPES and supplemented with 10% FBS), a parallel cell-containing well with the same maytansinoid concentration was prepared for each cell sample, with imaging medium replacing the regular culturing medium. This cell-containing coverslip was discarded, and the conditioned imaging medium was supplemented with 10 mmol/L DL-lactate and Oxyrase (1:50 final dilution; Oxyrase, Inc.) and then added to the cell sample to be imaged. Time-lapse images, between 30 and 38 frames at 4-second intervals, were taken over 1.5 hours (37 ± 1°C) with a 100× Nikon Plan Apo objective on a Nikon Eclipse E800 microscope (Nikon) with a CoolSNAP HQ2 camera (Roper Scientific GmbH) under the control of MetaMorph software (Molecular Devices). For each condition, the plus ends of 18 to 60 dynamic microtubules at the flat lamellar edges of interphase cells were tracked in MetaMorph software for ≥60 seconds, and the distances between an arbitrary microtubule origin point and the plus end were recorded as the microtubule lengths. To analyze dynamic instability, the lengths of individual microtubules were graphed versus elapsed time as life history plots. Microtubule dynamics were analyzed in IGOR Pro 6.0 software using the criteria described in refs. (33, 36). Briefly, changes of ≥0.5 μm were considered growth or shortening events. Changes of <0.5 μm were called pause (attenuation). The time-based catastrophe frequency is the number of catastrophes (transitions from growth or pause to shortening) divided by the total time spent growing and paused. The rescue frequency is the number of rescues (transitions from shortening to growth or pause) divided by the total time spent shortening. Dynamicity is the total length grown and shortened divided by the life span of the microtubules. Results are the means and SEM of at least three independent experiments.

Results

Maytansine, *S*-methyl DM1, and antibody-maytansinoid conjugates inhibit proliferation and arrest cells at mitosis

We measured the effects of maytansine, *S*-methyl DM1, and EpCAM-targeting disulfide-linked (B38.1-SPP-DM1) and thioether-linked (B38.1-SMCC-DM1) conjugates on proliferation of MCF7 cells over 72 hours (Fig. 2A). Both the unconjugated maytansinoids and the conjugated maytansinoids strongly inhibited cell proliferation in a concentration-dependent manner. The concentration dependence curves for the inhibition of cell proliferation by the unconjugated compounds (maytansine and *S*-methyl DM1) were sigmoidal in shape. Minimal inhibition occurred at 400 pmol/L maytansine and at 200 pmol/L *S*-methyl DM1, respectively, and inhibition was maximal at 6 and 3 nmol/L, respectively. For both immunoconjugates, minimal inhibition occurred at a concentration of 200 pmol/L, and inhibition increased gradually with increasing concentrations, attaining the maximum above 300 nmol/L. *S*-methyl DM1 (IC_{50} = 330 pmol/L) was slightly more potent than maytansine (IC_{50} = 710 pmol/L). Both AMCs had similar IC_{50} values (5.2 nmol/L for uncleavable B38.1-SMCC-DM1 and 11 nmol/L for cleavable B38.1-SPP-DM1). Thus, their potencies were between 1 and 2 orders of magnitude weaker than the unconjugated maytansinoids. Other studies have reported that the free and conjugated maytansinoids had similar IC_{50} values (32, 37). In the previous studies, the target antigens were expressed at much higher levels on the cells than the levels for the EpCAM antigen on the MCF-7 cells in the current study.

We determined the concentration dependence for G_2-M arrest at 24 hours of incubation (Fig. 2B) by flow cytometry of cells fixed and stained with propidium iodide (Materials and Methods). All four agents induced a maximum of 80% accumulation of cells in G_2-M compared with only 30% in controls (with no drug). The concentration dependence curves for G_2-M arrest paralleled the curves for inhibition of proliferation. Minimal G_2-M arrest with both maytansine and *S*-methyl DM1 occurred at 200 pmol/L, and arrest was maximal at 1 nmol/L, with half-maximal arrest occurring at 310 and 340 pmol/L, respectively. Minimal inhibition of G_2-M arrest with both conjugates occurred at 500 pmol/L, reaching the maximum at ≥100 nmol/L, with IC_{50} values of 7 nmol/L for

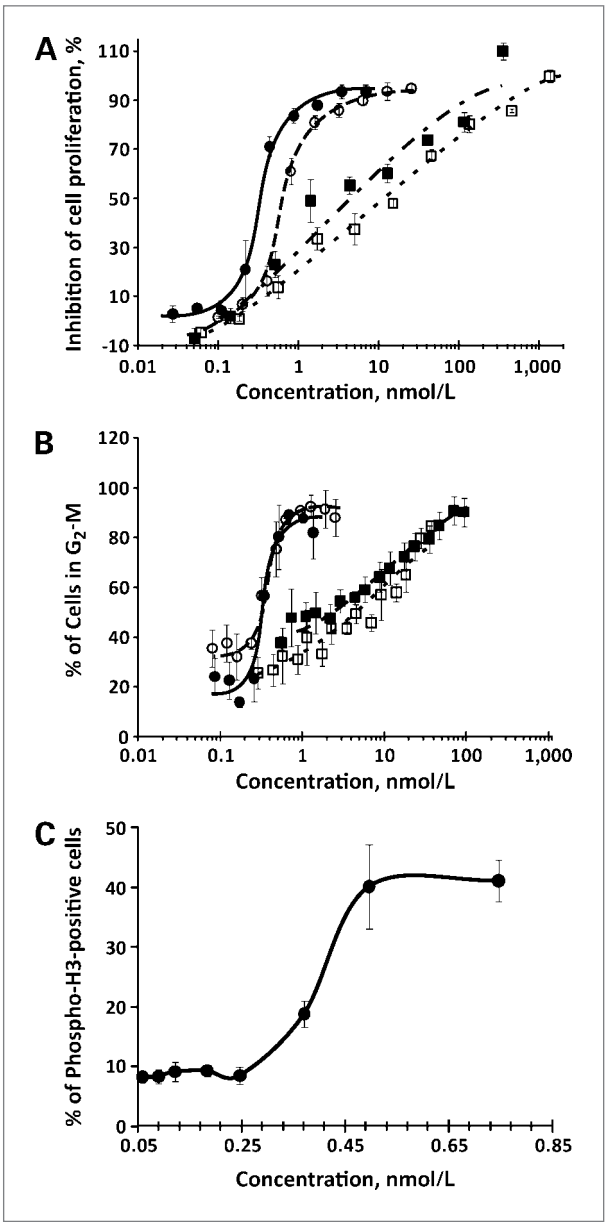

Figure 2. Concentration dependence for inhibition of proliferation (A), G_2-M arrest (B), and mitotic arrest of MCF7 cells by maytansinoids and their antibody conjugates (C). Cells were incubated with maytansine (○), *S*-methyl DM1 (●), B38.1-SPP-DM1 (□), and B38.1-SMCC-DM1 (■). A, cells were incubated with compound for 72 h, and inhibition of proliferation was measured by sulforhodamine B (Materials and Methods). Maytansine, *S*-methyl DM1, B38.1-SPP-DM1, and B38.1-SMCC-DM1 inhibited proliferation with IC_{50} values 710 pmol/L, 330 pmol/L, 11 nmol/L, and 5.2 nmol/L, respectively. B, cells were incubated with compounds for 24 h, and the population of G_2-M cells was determined by flow cytometry (Materials and Methods). Maytansine, *S*-methyl DM1, B38.1-SPP-DM1, and B38.1-SMCC-DM1 induced arrest in G_2-M with IC_{50} values 310 pmol/L, 340 pmol/L, 10 nmol/L, and 6.8 nmol/L, respectively. C, cells were incubated with *S*-methyl DM1 for 24 h, and the percentage of cells that stained positively for phosphorylated histone H3 was determined by flow cytometry or counted by microscopy (Materials and Methods). *S*-methyl DM1 induced mitotic arrest with an IC_{50} of 400 nmol/L. Results are means and SEM of at least three experiments.

B38.1-SMCC-DM1 and 10 nmol/L for B38.1-SPP-DM1. Arrest with *S*-methyl DM1 occurred specifically in mitosis as determined by immunostaining with antibodies against phosphorylated histone H3, a marker for mitotic cells. As shown in Fig. 2C, half-maximal mitotic arrest with *S*-methyl DM1 (IC_{50}, 0.4 nmol/L) occurred at the same concentration as G_2-M arrest.

The antibody specificity of the conjugate-induced cell cycle arrest was examined in two ways. Incubation of the cells with 11 nmol/L B38.1-SPP-DM1 in the presence of a 90-fold excess of unconjugated B38.1 antibody (1 μmol/L) induced no cell cycle arrest or inhibition of proliferation (data not shown). In addition, incubation of cells with Ab-SPP-DM1 and Ab-SMCC-DM1 conjugates that do not bind to any antigens on the MCF-7/GFP cells also induced no cell cycle arrest or inhibition of proliferation. These observations indicate that the activity of the B38.1-DM1 conjugates is antigen specific.

Effects of *S*-methyl DM1 on microtubule organization

To assess the effects of *S*-methyl DM1 on the microtubule network, cells were fixed and stained for microtubules, actin, and chromatin and examined by immunofluorescence microscopy (Materials and Methods). In control cells in the interphase, microtubules formed a fine filamentous network throughout the cell and actin formed a filamentous network at the cell periphery (Fig. 3A, a). After 24-hour incubation with 340 pmol/L *S*-methyl DM1 (the IC_{50} for mitotic arrest), some interphase cells were slightly rounded, but the microtubules and actin fibers in these cells (Fig. 3A, b) were indistinguishable from microtubules in control interphase cells.

At an *S*-methyl DM1 concentration of 680 pmol/L (2 × IC_{50}), the microtubules in interphase cells were shorter, fewer, and had a patchy distribution; small aggregates of tubulin were also apparent (Fig. 3A, c, arrowheads and arrows, respectively). The actin fiber network was unchanged. At 1.4 nmol/L *S*-methyl DM1 (4 × IC_{50}), no microtubules remained, most cells were rounded, and the actin occupied a narrow region at the cell periphery (Fig. 3A, d).

Mitotic spindle organization was examined in cells that were fixed and stained for microtubules, centrosomes, and chromatin. Control mitotic cells had well-separated centrosomes and well-formed bipolar spindles with only a few astral microtubules at the poles (Fig. 3B, e). All chromosomes in control metaphase spindles had congressed into a compact central metaphase plate.

The maytansinoids induced structural and functional spindle microtubule abnormalities at concentrations that induced little or no detectable change in the microtubule network of interphase cells. *S*-methyl DM1 at 1 × IC_{50} (340 pmol/L) induced striking abnormalities in mitotic cells (Fig. 3B, f–j). The majority had abnormal spindles classified as type I (Fig. 3B, f) or type II bipolar spindles, using the classification of Jordan et al. (38) and Ngan et al. (39), with more and longer astral microtubules than in spindles in control cells, some uncongressed chromosomes, and

reduced interpolar distances (data not shown; Fig. 3B, g, h). A few cells had spindles that were normal and bipolar with compact metaphase plates of congressed chromosomes, whereas a few mitotically arrested cells had type III abnormal ball-shaped spindles that were often monoastral, with little, if any, separation of the centrosomes (Fig. 3B, i,j). Chromosomes and star-like aggregates of thick microtubules surrounded the centrosomes.

S-methyl DM1 at 2 × mitotic IC_{50} to 4 × mitotic IC_{50} (680 pmol/L–1.4 nmol/L) induced predominantly type III spindles and increasing numbers of type IV abnormal spindles. In type IV abnormal spindles (Fig. 3B, k,l), only a few short thick microtubules surrounded unseparated or poorly separated centrosomes. There were frequent small tubulin aggregates and bundles of short microtubules that were not connected to the centrosomes. Interestingly,

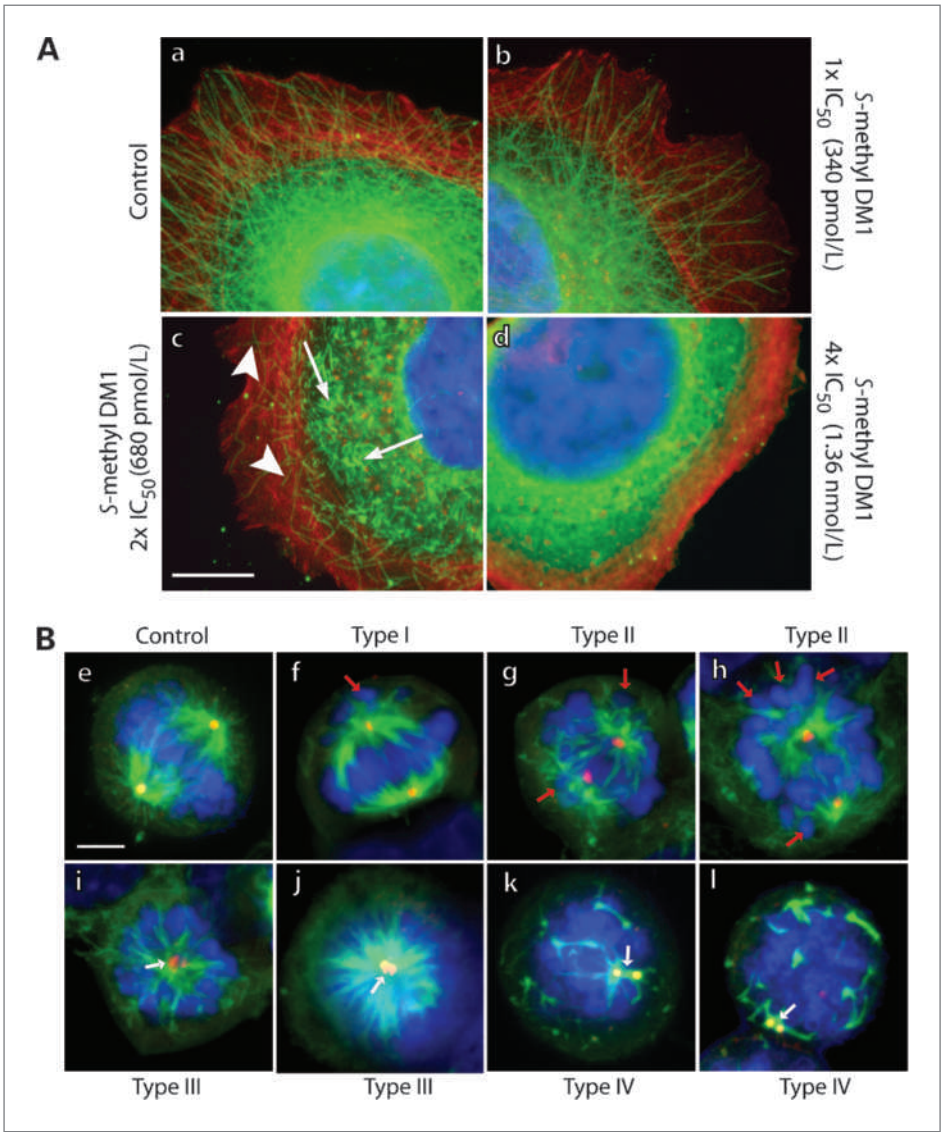

Figure 3. Effects of *S*-methyl DM1 on microtubule organization in interphase and mitosis. A, interphase: MCF7 cells were fixed and stained for α-tubulin (green), actin (red), and DNA (blue). Control cells (a) and cells treated for 24 h with 340 pmol/L (mitotic IC_{50}) *S*-methyl DM1 (b) show intact microtubule and actin networks with similar overall morphologies. At 680 pmol/L *S*-methyl DM1 (2× mitotic IC_{50}; c), microtubules were significantly shorter (arrowheads), reduced in number, and showed a patchy distribution. Some tubulin aggregates are visible (arrows). At 1.4 nmol/L *S*-methyl DM1 (4× mitotic IC_{50}; d), all microtubules were depolymerized and actin formed a narrow band at the cell periphery. Scale bar, 10 μm. B, mitosis: MCF7 cells were incubated for 24 h with medium alone (e) or with 340 pmol/L (1 × mitotic IC_{50}; f–j) or 680 pmol/L *S*-methyl DM1(2× mitotic IC_{50}; k, l). Cells were fixed and stained for α-tubulin (green), the centrosome-associated protein pericentrin (red), and DNA (blue). In control mitotic cells (e), spindles were normal with well-separated centrosomes and with the chromosomes congressed to a compact metaphase plate. The majority of cells arrested in mitosis by *S*-methyl DM1 displayed some abnormalities in metaphase: uncongressed chromosomes (red arrows), poorly defined bipolar spindles or monopolar spindles, an increased number of astral microtubules, and poorly separated centrosomes (white arrows). Based on these morphologic abnormalities, cells were categorized into type I, type II, type III, and type IV spindles (see Results). Scale bar, 5 μm.

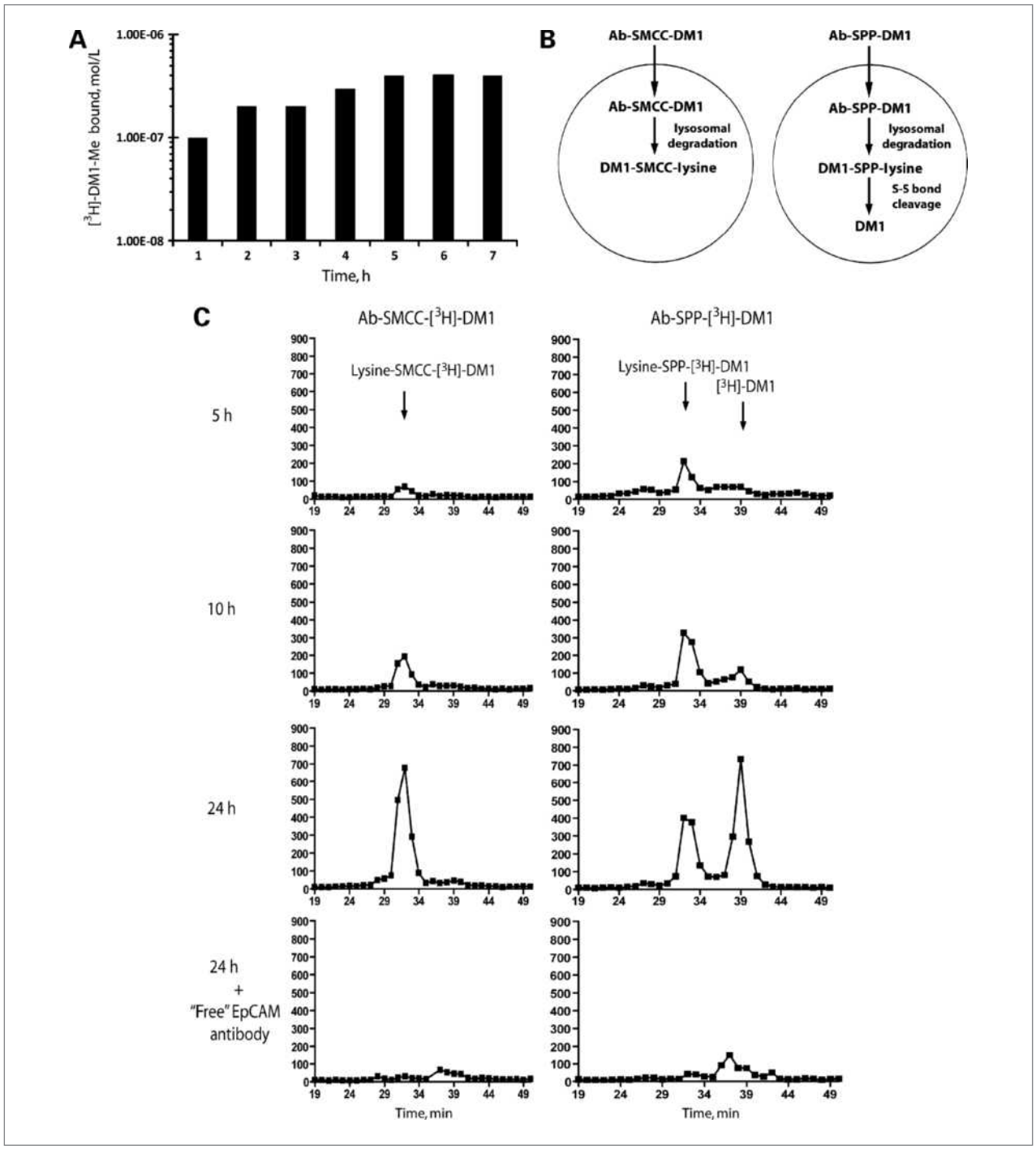

Figure 4. Comparison of the cellular accumulation of *S*-[^{3}H]methyl-DM1 with accumulation of the metabolites of cleavable and uncleavable anti-EpCAM antibody–[^{3}H]-DM1 conjugates. A, time course of uptake of 780 pmol/L [^{3}H]-*S*-methyl DM1 by MCF7 cells. B, diagram depicting the cellular uptake and processing of the anti-EpCAM antibody–DM1 conjugates, B38.1-SMCC-DM1 and B38.1-SPP-DM1. Both conjugates are internalized by antigen-mediated endocytotosis. The endosomes containing the conjugates fuse with lysosomes. The conjugates undergo proteolysis, forming the corresponding lysine-linker-maytansinoids, lysine-SMCC-DM1, and lysine-SPPDM1. The lysine-SPP-DM1 metabolite of the cleavable conjugate is further reduced to yield free DM1, whereas the lysine-SMCC-DM1 metabolite of the uncleavable conjugate resists additional processing. C, radiochromatograms of the [^{3}H]maytansinoid metabolites of B38.1-SPP-[^{3}H]DM1 and B38.1-SMCC-[^{3}H]DM1. MCF-7 cells were exposed to the anti-EpCAM antibody–[^{3}H]-DM1 conjugates for the indicated times. The homogenates were assayed for ^{3}H-maytansinoid metabolites by extraction and HPLC. The effluent from the samples was collected in 1 mL fractions, and the radioactivity corresponding to each fraction was determined by liquid scintillation counter. The counts per minute of tritium associated with the fractions were plotted versus the time the fraction was collected. The lowest two panels show that coincubation with 1 μmol/L unconjugated EpCAM antibody strongly inhibited the formation of the metabolites.

contrast to other microtubule-interacting compounds, no multipolar spindles occurred at any *S*-methyl DM1 concentration. Similar concentration-dependent changes in spindle organization occurred on treatment with free maytansine and the B38.1-DM1 conjugates (data not shown). Interestingly, the variety of abnormal spindles for any given concentration and the range of effects on interphase microtubules were greater with the immunoconjugates than with unconjugated maytansinoids, suggesting that the response varied significantly from cell to cell, perhaps due to variable uptake of the immunoconjugates resulting from variations in antigen density.

Cellular uptake of *S*-[^{3}H]methyl-DM1 and metabolism of B38.1-SMCC-[^{3}H]DM1 and B38.1-SPP-[^{3}H]DM1

We examined the time course for uptake of *S*-[^{3}H]methyl-DM1 into MCF7 cells. As shown in Fig. 4A, at a concentration of 780 pmol/L, *S*-[^{3}H]methyl-DM1 was taken up relatively rapidly, attaining an intracellular concentration of ~100 nmol/L at 1 hour and a concentration of 400 nmol/L at 5 hours.

To determine the time course for uptake and metabolism of the B38.1-DM1 conjugates, MCF7 cells were exposed to 10 nmol/L B38.1-SPP-[^{3}H]-DM1 or 10 nmol/L B38.1-SMCC-[^{3}H]-DM1 for 5, 9, or 24 hours. The cells were then analyzed for [^{3}H]maytansinoid metabolites by HPLC and liquid scintillation counting following acetone extraction (Fig. 4C). The observed metabolites had retention times identical to the target cell metabolites identified by liquid chromatography/mass spectrometry for the anti-CanAg conjugates, huC242-SPP-DM1, and huC242-SMCC-DM1 (26). At 5 and 10 hours, lysine-linker-maytansinoid adducts (DM1-SPP-lysine and DM1-SMCC-lysine) were the primary accumulated metabolites of the two conjugates. Even after a prolonged (24 hours) incubation of the cells with B38.1-SMCC-[^{3}H]-DM1 (Fig. 4C, left column), DM1-SMCC-lysine was the major metabolite. In contrast, the lysine-linker-maytansinoid adduct derived from the cleavable EpCAM-SPP-[^{3}H]-DM1 (Fig. 4C, right column) was accompanied at 10 hours by unconjugated DM1 that resulted from the intracellular reduction of the disulfide bond connecting the cross-linker and DM1. At 24 hours, similar levels of the cellular metabolites for the two conjugates formed as indicated by the areas under the peaks. This suggests that the rates for the initial steps through the lysosomal degradation shown in Fig. 4B are similar for the two conjugates. As shown in the bottom two panels of Fig. 4C, a 100-fold excess of unconjugated EpCAM antibody (1 μmol/L) significantly blocked cellular uptake and catabolism of the conjugates.

Maytansine and *S*-methyl DM1 suppress dynamic instability of microtubules in cells at concentrations that arrest mitosis

We examined the effects of free maytansinoids, *S*-methyl DM1 and maytansine, at their mitotic IC_{50} values, on dynamic instability of individual microtubules in MCF7 cells at 5-hour incubation, a time when the intracellular drug concentrations had attained equilibrium (Fig. 3A). Figure 5A shows representative frames from a time-lapse series of control cells and from cells incubated with 340 pmol/L *S*-methyl DM1, showing the changes in length of individual microtubules over time. The length changes were measured (Materials and Methods), and "life history plots" of the changes of the individual microtubules over time (Fig. 5B) were used to determine the parameters of dynamic instability (Table 1A). In control cells, most of the microtubules were dynamic, undergoing frequent transitions between relatively slow growth and rapid shortening. Plus ends of microtubules in control cells shortened at a rate of 20.0 ± 2.3 μm/min and grew at a rate of 12.9 ± 1.0 μm/min (Table 1A). They underwent catastrophes at a frequency of 2.3 ± 0.3/microtubule/min and transitioned to growth or attenuation from shortening (called rescue) at a frequency of 6.6 ± 0.5/microtubule/min. Their overall dynamicity (the total rate of exchange of tubulin with the microtubule end expressed as microtubule length per time) was 12.0 ± 0.6 μm/min.

In contrast, as shown in Table 1A, nearly half of the microtubules in cells incubated with either maytansine (310 pmol/L) or *S*-methyl DM1 (340 pmol/L; the mitotic IC_{50} values of the two drugs) were not dynamic; they did not grow or shorten detectably during the observation time. The dynamic instability of microtubules that retained dynamic behavior was significantly suppressed; they grew and shortened more slowly than microtubules in control cells. Maytansine had a somewhat stronger suppressive effect than *S*-methyl DM1 (Table 1A). The shortening rates were suppressed by maytansine and *S*-methyl DM1 by 45% and 22%, respectively, and the growth rates were suppressed by 37% and 28%, respectively. Maytansine and *S*-methyl DM1 suppressed the catastrophe frequency by 61% and 36%, respectively, and enhanced the rescue frequency by 19% and 68%, respectively. Dynamicity was suppressed 65% by maytansine and 58% by *S*-methyl DM1. The magnitude of suppression increased when the concentration of maytansine or *S*-methyl DM1 was increased from 1 × IC_{50} to 2 × IC_{50} (data not shown).

Antibody-maytansinoid (B38.1-DM1) conjugates suppress dynamic instability in parallel with intracellular metabolite formation

To determine whether the conjugate metabolites play a significant role in the antiproliferative and antimitotic mechanisms of the antibody-maytansinoid conjugates, we examined the relationship between metabolite formation and suppression of dynamic instability in the cells. Cells were incubated with 10 nmol/L B38.1-SMCC-DM1 or B38.1-SPP-DM1 for 5, 10, and 24 hours. This concentration approximates the antimitotic IC_{50} values of the immunoconjugates (7 nmol/L for the uncleavable B38.1-SMCC-DM1 and 10 nmol/L for the cleavable B38.1-SPP-DM1;

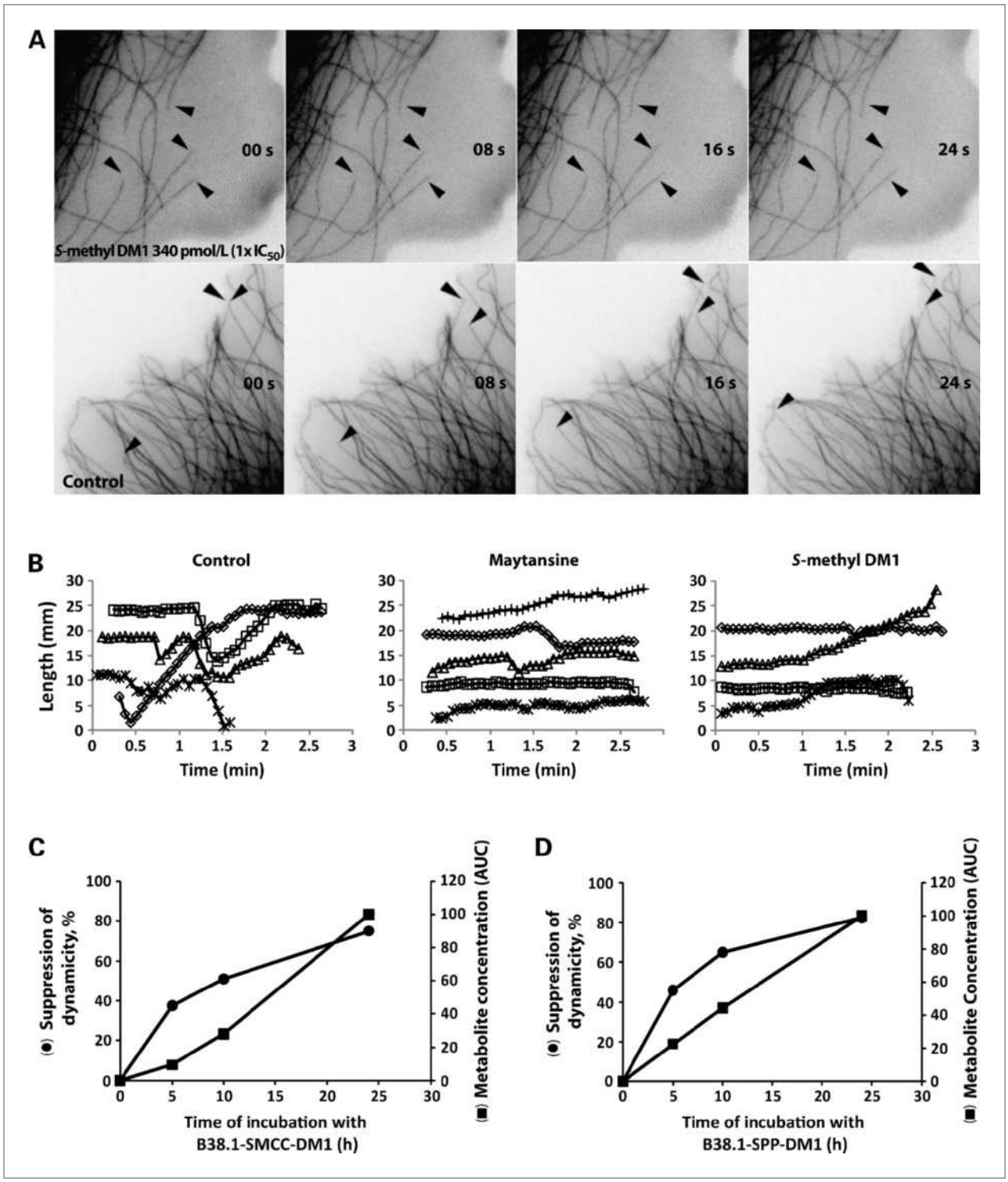

Figure 5. Dynamic instability of microtubules in MCF7 cells incubated with maytansine, *S*-methyl DM1, B38.1-SMCC-DM1, and B38.1-SPP-DM1. Cells were incubated for 5 h with 310 pmol/L maytansine, 340 pmol/L *S*-methyl DM1, 10.5 nmol/L B38.1-SPP-DM1, and 6.8 nmol/L B38.1-SMCC-DM1 (1 × IC_{50} concentrations of the corresponding compounds) or medium alone. A, time-lapse images of individual microtubules in the lamellar periphery of cells were recorded by epifluorescence microscopy. Microtubule ends (▲) were tracked over time to produce life history plots. B, life history plots of length of individual microtubules. In all cells treated with maytansinoids, the dynamic instability of individual microtubules was visibly suppressed. Over the 24-h time course of incubation with B38.1-SMCC-DM1 (C) and B38.1-SPP-DM1 (D), suppression of microtubule dynamicity (left axes) increased similarly with the increase in the intracellular concentration of the metabolite of the B38.1-DM1 conjugates as determined by the AUC (area under the curve; right axes) as shown in Fig. 4C.

Table 1. Suppression of MT dynamic instability in MCF7 cells incubated with maytansine, S-methyl DM1, B38.1-SMCC-DM1, and B38.1-SPP-DM1

A. Suppression of MT dynamic instability in MCF7 cells by maytansine and *S*-methyl DM1 after 5-h incubation with cell cycle 1 × IC_{50} concentrations

MT dynamic instability parameters	Control	*S*-methyl DM1 (340 pmol/L)	% change	Maytansine (310 pmol/L)	% Change
Growth rate, μm/min	12.9 ± 1.0	9.9 ± 1.2**	–22	6.9 ± 0.5**	–45
Shortening rate, μm/min	20.0 ± 2.3	14.3 ± 1.6**	–28	12.5 ± 1.3**	–37
% Time spent growing	51	27	–47	30	–41
% Time spent shortening	26	14	–45	11	–58
% Time spent attenuated	23	59	157	59	158
Catastrophe frequency, no./MT/min	2.5 ± 0.3	1.6 ± 0.2 *	–36	1.0 ± 0.1**	–61
Rescue frequency, no./MT/min	6.6 ± 0.5	11.0 ± 0.7**	68	7.8 ± 0.6	19
Growth distance, no./MT/μm	0.36 ± 0.06	0.77 ± 0.20	113	0.49 ± 0.07	35
Shortening distance, no./MT/μm	0.35 ± 0.04	1.11 ± 0.11**	213	0.83 ± 0.10**	136
Dynamicity	12.0 ± 0.6	5.0 ± 0.6**	–58	4.3 ± 0.3**	–65
Nondynamic MT	5%	45%		48%	

B. Time dependence for suppression of MT dynamic instability in MCF7 cells by 10 nmol/L B38.1-SMCC-DM1

MT dynamic instability parameters	Control	5 h	% Change	10 h	% Change	24 h	% Change
Growth rate, μm/min	12.9 ± 1.0	11.4 ± 1.2	–10	11.7 ± 1.6	–8	6.95 ± 0.5**	–45
Shortening rate, μm/min	20.0 ± 2.3	13.6 ± 1.2**	–31	13.7 ± 2.4**	–31	11.0 ± 1.0**	–45
% Time spent growing	51	43	–16	39	–24	17	–67
% Time spent shortening	26	15	–41	9	–65	7	–74
% Time spent attenuated	23	42	83	52	130	76	235
Catastrophe frequency, no./MT/min	2.5 ± 0.3	1.3 ± 0.1**	–48	1.1 ± 0.2**	–55	1.2 ± 0.1**	–50
Rescue frequency, no./MT/min	6.6 ± 0.5	8.1 ± 0.5	23	10.4 ± 1.0**	58	10.6 ± 0.9**	62
Growth distance, no./MT/μm	0.36 ± 0.06	0.40 ± 0.06	11	0.39 ± 0.08	7	1.00 ± 0.14**	173
Shortening distance, no./MT/μm	0.35 ± 0.04	0.69 ± 0.06**	95	1.03 ± 0.2**	192	1.17 ± 0.14**	232
Dynamicity	12.0 ± 0.6	7.5 ± 0.6**	–37	5.9 ± 0.9**	–51	3.0 ± 0.3**	–75
Nondynamic MT	5%	6%		17%		44%	

C. Time dependence for suppression of MT dynamic instability in MCF7 cells by 10 nmol/L B38.1-SPP-DM1

MT dynamic instability parameters	Control	5 h	% Change	10 h	% Change	24 h	% Change
Growth rate, μm/min	12.9 ± 1.0	10.5 ± 0.7**	–17	9.9 ± 0.8**	–22	6.4 ± 0.6**	–50
Shortening rate, μm/min	20.0 ± 2.3	14.4 ± 1.3**	–28	12.3 ± 1.4**	–38	7.8 ± 1.0**	–61
% Time spent growing	51	31	–39	26	–50	24	–52
% Time spent shortening	26	21	–21	11	–56	5	–82
% Time spent attenuated	23	48	111	63	176	71	211
Catastrophe frequency, no./MT/min	2.5 ± 0.3	1.9 ± 0.1*	–25	1.2 ± 0.1**	–51	0.6 ± 0.1**	–75
Rescue frequency, no./MT/min	6.6 ± 0.5	7.1 ± 0.5	9	9.6 ± 0.7**	46	10.9 ± 1.2*	67
Growth distance, no./MT/μm	0.36 ± 0.06	0.66 ± 0.09*	79	0.75 ± 0.10**	104	0.95 ± 0.35	160
Shortening distance, no./MT/μm	0.35 ± 0.04	0.63 ± 0.06**	79	1.08 ± 0.10**	207	1.70 ± 0.26**	382
Dynamicity	12.0 ± 0.6	6.49 ± 0.5**	–46	4.2 ± 0.4**	–65	2.1 ± 0.3**	–83
Nondynamic MT	5%	20%		42%		38%	

NOTE: For A, cells were incubated for 5 h with maytansine or *S*-methyl DM1 at G_2-M arrest 1 × IC_{50} concentrations (310 and 340 pmol/L, respectively) before time-lapse microscopy. For B38.1-SMCC-DM1 (B) and B38.1-SPP-DM1 (C), cells were incubated with 10 nmol/L of AMC for the indicated periods of time before time-lapse microscopy. Results presented are average values ± SEM as well as the corresponding percentage of change from control. Values with ** are significantly different from control at ≥99% confidence interval, and values with * are significantly different from control at ≥95% confidence interval by Student's *t* test. Values for percentage of time spent in growth, shortening, and attenuation were calculated for the entire population of microtubules and, thus, the confidence intervals for these parameters cannot be computed.

Abbreviation: MT, microtubule.

Fig. 2B) and is the same concentration used in the uptake and metabolism study (Fig. 4C). Incubation with either immunoconjugate for 5 hours moderately suppressed microtubule dynamic instability; the suppressive effects increased at 10 and 24 hours (Table 1B and C). Similar to *S*-methyl DM1 and maytansine, incubation with B38.1-SMCC-DM1 and B38.1-SPP-DM1 for 5 hours reduced growth rates by 10% and 17%, respectively; shortening rates by 31% and 28%, respectively; and catastrophe frequencies by 48% and 25%, respectively. As shown in Fig. 5C and Table 1B, the suppressive effects on dynamic instability were proportional to the increase in intracellular concentration of the metabolites, attaining 45% and 50% suppression of growth rates, 45% and 61% suppression of shortening rates, and 50% and 75% suppression of the catastrophe frequency for the two immunoconjugates, respectively, at 24-hour incubation. The overall dynamicity at 5 hours was suppressed by 37% and 46% by B38.1-SMCC-DM1 and B38.1-SPP-DM1, respectively, and increased to 75% and 83%, respectively, at 24 hours. The time dependence for inhibition of dynamicity compared with the appearance of the metabolites is shown in Fig. 5. Thus, the cleavable and uncleavable B38.1-DM1 conjugates both disrupt the microtubule dynamic instability in concert with the cellular accumulation of their metabolites. As a control, we added a 100-fold excess of unconjugated B38.1 antibody (1 μmol/L) simultaneously with the conjugates. This completely prevented suppression of microtubule dynamic instability (data not shown), indicating that antibody-mediated uptake of the B38-DM1 conjugates is required to suppress dynamic instability.

Discussion

We found that maytansine, *S*-methyl DM1, and the anti-EpCAM antibody-maytansinoid conjugates B38.1-SPP-DM1 and B38.1-SMCC-DM1 all inhibited the proliferation of MCF7 cells at subnanomolar or nanomolar concentrations in concert with mitotic arrest and suppression of microtubule dynamic instability. Internalization and metabolism of the conjugates led to continued potent suppression of dynamic instability, indicating that the metabolites and the free unconjugated maytansinoids exert their potent antimitotic effects through a common mechanism involving suppression of microtubule dynamic instability.

Proliferation

We found that maytansine, *S*-methyl DM1, and the anti-EpCAM conjugates B38.1-SPP-DM1 and B38.1-SMCC-DM1 all inhibited proliferation of MCF7 cells with IC_{50} values of 710 pmol/L for maytansine, 330 pmol/L for *S*-methyl DM1, 5.2 nmol/L for B38.1-SPP-DM1, and 11 nmol/L for B38.1-SMCC-DM1. The differences in potency between the conjugates and the free maytansinoids may be attributed to the relatively low expression of the EpCAM antigen on the MCF7 cells. Indeed, the B38.1-SMCC-DM1 conjugate was shown to be much more cytotoxic toward other carcinoma cells than is reported here with MCF7 cells, presumably due to the higher levels of the EpCAM antigen on the other cells (40). Also, in a related study, the cytotoxic potencies of CanAg-targeting antibody maytansinoid conjugates toward cell lines with high levels of the target antigen were found to be similar to the potencies of the free maytansine and *S*-methyl DM1 (26, 32). We found that the concentration-response curves for the free maytansinoids were steep and S-shaped, whereas the response curves for both conjugates were more linear and increased relatively slowly. This difference in response most likely results from the different mechanisms of cellular uptake for free and conjugated maytansinoids and from the relatively low expression level of the EpCAM antigen on the MCF-7 cells compared with the expression of human epidermal growth factor receptor 2 in previous studies with the trastuzumab-DM1 conjugate (32, 37).

Inhibition of proliferation occur in concert with mitotic arrest

G_2-M arrest was induced half-maximally for each compound at a concentration that was similar to the concentration that inhibited proliferation by 50% (half-maximal G_2-M arrest at 310 pmol/L maytansine, 340 pmol/L *S*-methyl DM1, 6.8 nmol/L B38.1-SMCC-DM1, and 10.5 nmol/L B38.1-SPP-DM1). Staining of cells by 4′,6-diamidino-2-phenylindole and phosphohistone-H3 antibody indicated that mitotic arrest occurred predominantly in prometaphase/metaphase of mitosis and that the drugs induced significant drug concentration–dependent abnormalities in the arrested spindles. Thus, inhibition of proliferation occurred by mitotic arrest. Interphase microtubule arrays were normal except at high drug concentrations (2–4 × IC_{50}) at which microtubules were depolymerized and some tubulin accumulations or aggregates were formed.

The maytansinoid-induced spindle abnormalities were strikingly similar to those induced by other microtubule-interacting compounds, including *Vinca* alkaloids, 2-methoxyestradiol, taxanes, podophyllotoxin, nocodazole, sulforaphane, and eribulin (35, 38, 39, 41). The abnormalities included a concentration-dependent increase in the number of uncongressed chromosomes, an increase in the number of astral microtubules, and a shortened pole-to-pole distance. At very high concentrations, spindles were monopolar with a spherical central accumulation of condensed chromosomes and star-shaped aggregates of short, thick microtubules. The failure of congression is likely due to the inability of both kinetochores of sister chromosomes to secure proper attachments to microtubules from opposite poles due to the suppressed dynamic instability of spindle microtubules. The shortened pole-to-pole distance is also likely due to suppression

of microtubule dynamics and/or to some microtubule depolymerization. Interestingly, we observed no multipolar spindles, suggesting that centrosomal duplication or integrity was unaffected.

Antibody-maytansinoid conjugates (B38.1-SPP-DM1 and B38.1-SMCC-DM1) are internalized in an antigen-specific manner and metabolized

Because we found that an excess of unconjugated antibody prevented internalization of both the cleavable and uncleavable B38.1-DM1 conjugates, it is clear that they were internalized by cells in an antigen-specific manner. The lysine adduct produced by metabolism of the uncleavable B38.1-SMCC-DM1 (Lys-SMCC-DM1) was detected in the cells after 5 hours of incubation, and the quantity continued to increase after 10 and 24 hours of incubation. Although the analogous lysine-SPP-DM1 metabolite of the B38.1-SPP-DM1 conjugate was observed in cells at 5 hours and increased in quantity at 10 hours, it underwent an additional reduction to yield DM1 itself at 24 hours. The appearance of the Lys-SPP-DM1 metabolite before DM1 indicates that lysosomal degradation of the antibody component preceded reduction of the disulfide bond in the chemical linker to produce DM1. These findings are in concert with previous studies on metabolism of cleavable and uncleavable antibody-maytansinoid conjugates (25).

Maytansinoids suppress dynamic instability similarly in cells and with purified microtubules *in vitro*

The characteristics of maytansinoid-induced suppression of dynamic instability in cells are similar in most respects, qualitatively and quantitatively, to results on the suppressive effects of maytansine and *S*-methyl DM1 on dynamic instability of purified bovine brain microtubules reported in the accompanying article (30). For example, 340 pmol/L *S*-methyl DM1 added to MCF7 cells suppressed microtubule growth rates by 22%, compared with 24% suppression by 100 nmol/L *S*-methyl DM1 with purified microtubules. Similarly, shortening rates were suppressed by 28% and 67%, respectively; the catastrophe frequency was suppressed by 36% and 90%, respectively; and overall dynamicity was suppressed by 58% and 84%, respectively.

Comparing the intracellular concentration of *S*-methyl DM1 with the concentration that was added to the medium indicated that the intracellular concentration increased about 500-fold. (Addition of 780 pmol/L *S*-methyl DM1 to the cells resulted in an intracellular concentration of 400 nmol/L; Fig. 4A.) A similar cellular uptake phenomenon is frequently observed with other microtubule-targeted drugs (42, 43). From these data, we estimate that the addition of 340 pmol/L *S*-methyl DM1 to the cells would have resulted in an intracellular concentration of ~80 nmol/L *S*-methyl DM1, similar to the concentration of 100 nmol/L that was used *in vitro* with purified microtubules. Thus, the effective concentrations in cells and *in vitro* with purified microtubules are similar.

The only significant difference between the dynamics results in cells and *in vitro* was that the rescue frequency was affected in opposite ways in the two environments. It was reduced by 44% by 100 nmol/L *S*-methyl DM1 with purified microtubules, whereas it was increased 68% by 340 pmol/L *S*-methyl DM1 in cells. A possible explanation for this difference is that microtubule tips that are not capped by GTP-tubulin but instead have exposed GDP-tubulin at their tips are thought to have an unstable conformation that can undergo rapid microtubule depolymerization. Rescue of such a rapid shortening or depolymerization event may occur at microtubule regions where tubulin with bound GTP or with a GTP-like conformation exist in the body of the microtubule (44). It is conceivable that in the complex milieu of the cell, maytansine, or *S*-methyl DM1 interacts with some of the many proteins that associate with microtubules (microtubule-associated proteins, protein motors, etc.) and thereby prevents some regions of the microtubule from completing GTP hydrolysis or from attaining the unstable GDP-associated conformation, thus increasing the rescue frequency; however, *in vitro* with purified microtubules and no microtubule-associated proteins, such stabilized regions may not exist.

In all respects except for the opposite effects on rescue frequency, the *in vitro* results are similar to the results reported for cells (Table 1), indicating that the maytansinoid mechanisms in the complex milieu of the cell are similar to those *in vitro*. Thus, both in cells and *in vitro*, at low concentrations (those that induce mitotic arrest), it seems that maytansinoids stabilize microtubule dynamics by suppressing microtubule growth and shortening and catastrophe by binding with high affinity to a few sites at microtubule ends (30). At higher concentrations, the maytansinoids depolymerize microtubules both *in vitro* and in cells.

Metabolites suppress dynamic instability similarly to the unconjugated compound, in concert with their cellular accumulation

Like the free maytansinoids, the cleavable and uncleavable B38.1-DM1 conjugates and their metabolites inhibited cell proliferation and arrested cells in mitosis by suppressing microtubule dynamic instability. Dynamic instability was significantly inhibited by the low levels of metabolites produced at 5 hours of incubation, and inhibition increased significantly after 10 and 24 hours incubation (Table 1; Fig. 5). At the concentrations that induced half-maximal G_2-M arrest, the conjugates suppressed or enhanced the same microtubule dynamic parameters to similar degrees and in similar directions as free *S*-methyl DM1 and maytansine. Both growth and shortening rates, the catastrophe frequency, and dynamicity were suppressed by all four maytansinoids, and the rescue frequency was enhanced. As shown in Fig. 5C

and D, the time dependence for increased effects on microtubule dynamicity paralleled the increase in intracellular metabolite concentration arising from metabolism of B38.1-SMCC-DM1. For the cleavable B38.1-SPP-DM1, the time dependence for the sum of the concentrations of the two metabolites approximately paralleled the time dependence for increase in suppression of microtubule dynamicity. Thus, the results indicate that the metabolites and the free unconjugated maytansinoids have similar mechanisms of action, exerting their antiproliferative effects by inhibiting mitosis through suppression of microtubule dynamic instability.

Disclosure of Potential Conflicts of Interest

The laboratory of the corresponding author (M.A. Jordan) received a gift from ImmunoGen, Inc., in partial support of this work.

Grant Support

USPHS CA 57291 and NS13560.
The costs of publication of this article were defrayed in part by the payment of page charges. This article must therefore be hereby marked *advertisement* in accordance with 18 U.S.C. Section 1734 solely to indicate this fact.

Received 07/08/2010; revised 08/09/2010; accepted 08/18/2010; published 10/11/2010.

References

1. Kupchan SM, Komoda Y, Branfman AR, et al. The maytansinoids. Isolation, structural elucidation, and chemical interrelation of novel ansa macrolides. J Org Chem 1977;42:2349–57.
2. Kupchan SM, Komoda Y, Court WA, et al. Maytansine, a novel antileukemic ansa macrolide from *Maytenus ovatus*. J Am Chem Soc 1972;94:1354–6.
3. Kupchan SM, Sneden AT, Branfman AR, et al. Structural requirements for antileukemic activity among the naturally occurring and semisynthetic maytansinoids. J Med Chem 1978;21:31–7.
4. Sieber SM, Wolpert MK, Adamson RH, Cysyk RL, Bono VH, Johns DG. Experimental studies with maytansine—a new antitumor agent. Bibl Haematol 1975:495–500.
5. Wolpert-DeFilippes MK, Bono VH, Jr., Dion RL, Johns DG. Initial studies on maytansine-induced metaphase arrest in L1210 murine leukemia cells. Biochem Pharmacol 1975;24:1735–8.
6. Bhattacharyya B, Wolff J. Maytansine binding to the vinblastine sites of tubulin. FEBS Lett 1977;75:159–62.
7. Mandelbaum-Shavit F, Wolpert-DeFilippes MK, Johns DG. Binding of maytansine to rat brain tubulin. Biochem Biophys Res Commun 1976;72:47–54.
8. Sieber SM, Mead JA, Adamson RH. Pharmacology of antitumor agents from higher plants. Cancer Treat Rep 1976;60:1127–39.
9. Remillard S, Rebhun LI, Howie GA, Kupchan SM. Antimitotic activity of the potent tumor inhibitor maytansine. Science (New York, NY) 1975;189:1002–5.
10. Huang AB, Lin CM, Hamel E. Maytansine inhibits nucleotide binding at the exchangeable site of tubulin. Biochem Biophys Res Commun 1985;128:1239–46.
11. Issell BF, Crooke ST. Maytansine. Cancer Treat Rev 1978;5:199–207.
12. Chari RV. Targeted cancer therapy: conferring specificity to cytotoxic drugs. Acc Chem Res 2008;41:98–107.
13. Ricart AD, Tolcher AW. Technology insight: cytotoxic drug immunoconjugates for cancer therapy. Nat Clin Pract 2007;4:245–55.
14. Kovtun YV, Goldmacher VS. Cell killing by antibody-drug conjugates. Cancer Lett 2007;255:232–40.
15. Wu AM, Senter PD. Arming antibodies: prospects and challenges for immunoconjugates. Nature Biotechnol 2005;23:1137–46.
16. Lambert JM. Drug-conjugated monoclonal antibodies for the treatment of cancer. Current Opin Pharmacol 2005;5:543–9.
17. Chari RV, Martell BA, Gross JL, et al. Immunoconjugates containing novel maytansinoids: promising anticancer drugs. Cancer Res 1992; 52:127–31.
18. Liu C, Tadayoni BM, Bourret LA, et al. Eradication of large colon tumor xenografts by targeted delivery of maytansinoids. Proc Natl Acad Sci U S A 1996;93:8618–23.
19. Kovtun YV, Audette CA, Ye Y, et al. Antibody-drug conjugates designed to eradicate tumors with homogeneous and heterogeneous expression of the target antigen. Cancer Res 2006;66:3214–21.
20. Tolcher AW, Ochoa L, Hammond LA, et al. Cantuzumab mertansine, a maytansinoid immunoconjugate directed to the CanAg antigen: a phase I, pharmacokinetic, and biologic correlative study. J Clin Oncol 2003;21:211–22.
21. Tijink BM, Buter J, de Bree R, et al. A phase I dose escalation study with anti-CD44v6 bivatuzumab mertansine in patients with incurable squamous cell carcinoma of the head and neck or esophagus. Clin Cancer Res 2006;12:6064–72.
22. Helft PR, Schilsky RL, Hoke FJ, et al. A phase I study of cantuzumab mertansine administered as a single intravenous infusion once weekly in patients with advanced solid tumors. Clin Cancer Res 2004;10: 4363–8.
23. Krop IE, Beeram M, Modi S, et al. Phase I study of trastuzumab-DM1, an HER2 antibody-drug conjugate, given every 3 weeks to patients with HER2-positive metastatic breast cancer. J Clin Oncol 2010;28:2698–704.
24. Smith SV. Technology evaluation: huN901-1, ImmunoGen. Curr Opin Mol Ther 2005;7:394–401.
25. Erickson HK, Park PU, Widdison WC, et al. Antibody-maytansinoid conjugates are activated in targeted cancer cells by lysosomal degradation and linker-dependent intracellular processing. Cancer Res 2006;66:4426–33.
26. Erickson HK, Widdison WC, Mayo MF, et al. Tumor delivery and *in vivo* processing of disulfide-linked and thioether-linked antibody-maytansinoid conjugates. Bioconjug Chem 2010;21:84–92.
27. Jordan MA, Wilson L. Microtubules as a target for anticancer drugs. Nature Rev 2004;4:253–65.
28. Jordan MA, Kamath K. How do microtubule-targeted drugs work? An overview. Curr Cancer Drug Targets 2007;7:730–42.
29. Jordan MA. Mechanism of action of antitumor drugs that interact with microtubules and tubulin. Curr Med Chem 2002;2:1–17.
30. Lopus M, Oroudjev E, Wilson L, et al. Maytansine and Cellular Metabolites of Antibody-Maytansinoid Conjugates Strongly Suppress Microtubule Dynamics by Binding to Microtubules. Mol Cancer Ther 2010;9:2689–99.
31. Xie H, Audette C, Hoffee M, Lambert JM, Blattler WA. Pharmacokinetics and biodistribution of the antitumor immunoconjugate, cantuzumab mertansine (huC242-1), and its two components in mice. J Pharmacol Exp Ther 2004;308:1073–82.
32. Widdison WC, Wilhelm SD, Cavanagh EE, et al. Semisynthetic maytansine analogues for the targeted treatment of cancer. J Med Chem 2006;49:4392–408.
33. Kamath K, Jordan MA. Suppression of microtubule dynamics by epothilone B is associated with mitotic arrest. Cancer Res 2003; 63:6026–31.
34. Skehan P, Storeng R, Scudiero D, et al. New colorimetric cytotoxicity assay for anticancer-drug screening. J Natl Cancer Inst 1990;82: 1107–12.
35. Kamath K, Okouneva T, Larson G, Panda D, Wilson L, Jordan MA. 2-Methoxyestradiol suppresses microtubule dynamics and arrests mitosis without depolymerizing microtubules. Mol Cancer Ther 2006;5: 2225–33.
36. Kamath K, Oroudjev E, Jordan MA. Determination of microtubule dynamic instability in living cells. In: Cassimeris L, Phong T, editors. Methods in cell biology. Philadelphia: Elsevier; 2010, p. 1–14.
37. Lewis Phillips GD, Li G, Dugger DL, et al. Targeting HER2-positive

breast cancer with trastuzumab-DM1, an antibody-cytotoxic drug conjugate. Cancer Res 2008;68:9280–90.
38. Jordan MA, Thrower D, Wilson L. Mechanism of inhibition of cell proliferation by *Vinca* alkaloids. Cancer Res 1991;51:2212–22.
39. Ngan VK, Bellman K, Hill BT, Wilson L, Jordan MA. Mechanism of mitotic block and inhibition of cell proliferation by the semisynthetic *Vinca* alkaloids vinorelbine and its newer derivative vinflunine. Mol Pharmacol 2001;60:225–32.
40. Kovtun YV, Audette CA, Mayo MF, et al. Antibody-maytansinoid conjugates designed to bypass multidrug resistance. Cancer Res 2010;70:2528–37.
41. Azarenko O, Okouneva T, Singletary KW, Jordan MA, Wilson L. Suppression of microtubule dynamic instability and turnover in MCF7 breast cancer cells by sulforaphane. Carcinogenesis 2008; 29:2360–8.
42. Jordan MA, Wilson L. The use and action of drugs in analyzing mitosis. Methods in cell biology. Academic Press; 1999, p. 267–95.
43. Jordan MA, Wilson L. The use of drugs to study the role of microtubule assembly dynamics in living cells. In: Vallee R, editor. Molecular motors and the cytoskeleton, methods in enzymology. San Diego: Academic Press; 1998, p. 252–76.
44. Dimitrov A, Quesnoit M, Moutel S, Cantaloube I, Pous C, Perez F. Detection of GTP-tubulin conformation *in vivo* reveals a role for GTP remnants in microtubule rescues. Science (New York, NY) 2008;322:1353–6.